Integration of Multiscale Material Models, Uncertainty Quantification and Characterization Techniques to Establish PSP Relations in Polycrystalline Materials

Saikumar R. Yeratapally[1], Patrick E. Leser[2], Christapher G. Lang[2], Albert Cerrone[3], William P. Leser[2], Geoffrey F. Bomarito[2], John A. Newman[2], Patricia Howell[2], Vesselin Yamakov[1], Brodan Richter[2]

[1]National Institute of Aerospace, Hampton, VA

[2]NASA Langley Research Center, Hampton, VA

[3]University of Notre Dame, Notre Dame, IN

TIM with Los Alamos National Laboratory

July 21st, 2020

OUTLINE

- Introduction
- Process-Structure-Property (PSP) Framework
- Effect-of-Defects Study
- Porosity Prediction Framework
- Uncertainty Quantification
- Physics-based Simulations

INTRODUCTION: PSP Relations

Atomic structure

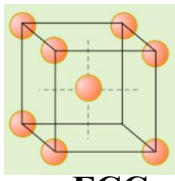

Microstructure

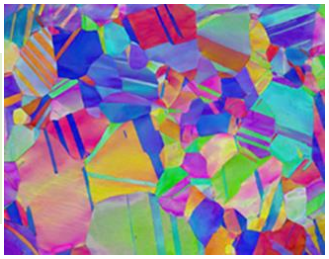

Credit: Hikari

Defect structure

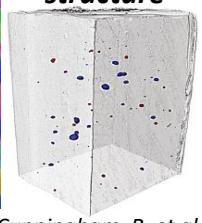

Cunningham, R. et al.

Turbine disk

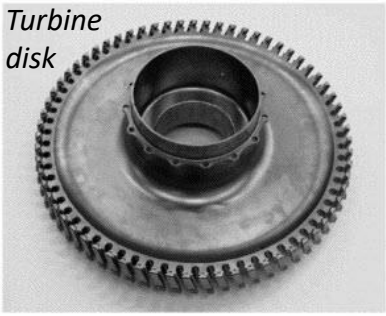

Credit: public domain

Process → Structure → Property/Performance

BOTTOM-UP *(using high-fidelity models)*

TOP-DOWN (using reduced-order models)

Processing → Structure → Properties → Performance

INTRODUCTION: SLM Process

Selective Laser Melting (SLM): An additive manufacturing (AM) technique that uses a high-power density laser to melt and fuse metallic powders together into a 3D component

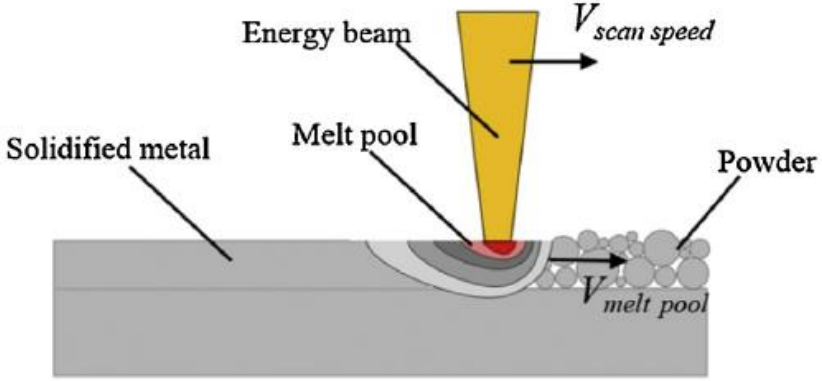

H. Gong et al. / Additive Manufacturing 1–4 (2014) 87–98

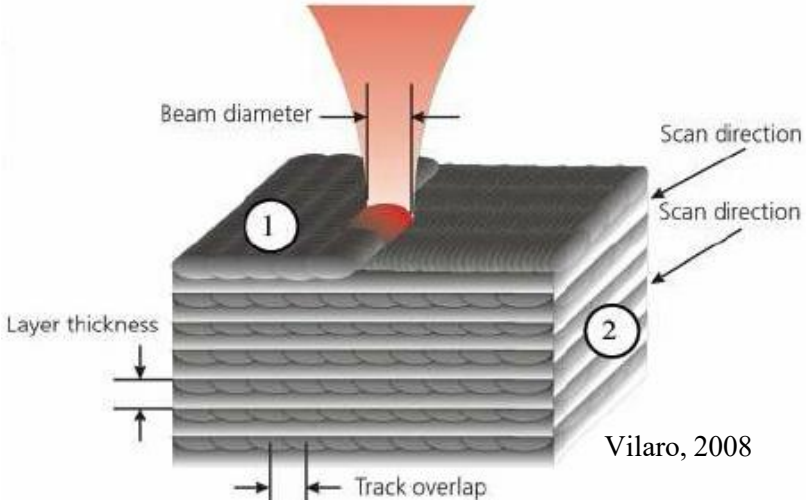

Vilaro, 2008

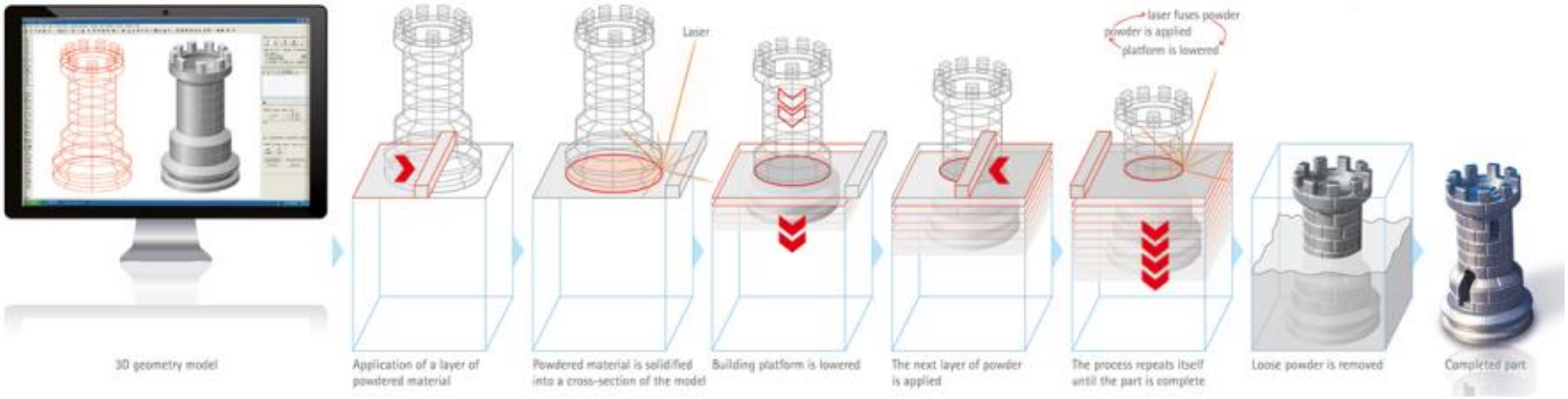

INTRODUCTION: SLM Design Space

Machine Parameters		Manufacturing Parameters		Feedstock Properties	
Laser Power	Chamber Atmosphere	Part Geometry	Part Orientation	Composition	Powder Shape
Laser Speed	Chamber Airflow	Scan Strategy	Support Structures	Avg Powder Size	Thermal Properties
Laser Spot Size	Build Plate Properties	Feature Size	Local Properties	Powder Size Distribution	Recycled
Hatch Spacing	Powder Bed Temperature				
Layer Thickness	Layer Rotation				

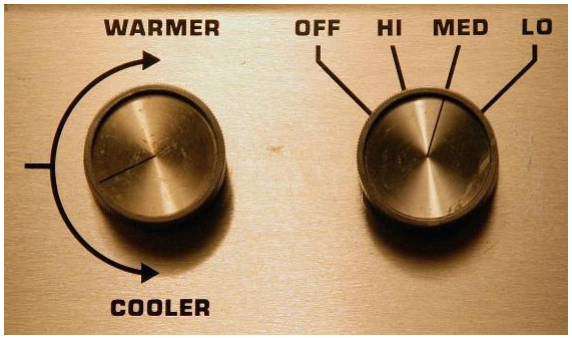

INTRODUCTION: Defects in SLM Process

Keyhole porosity

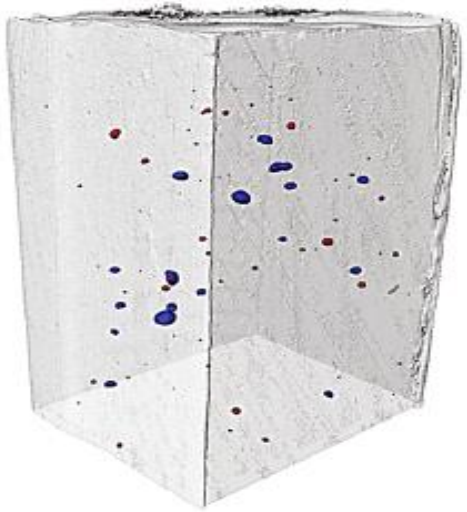

Cunningham, R. et al. JOM, Vol. 69, No. 3, 2017

Lack of fusion (LoF) porosity

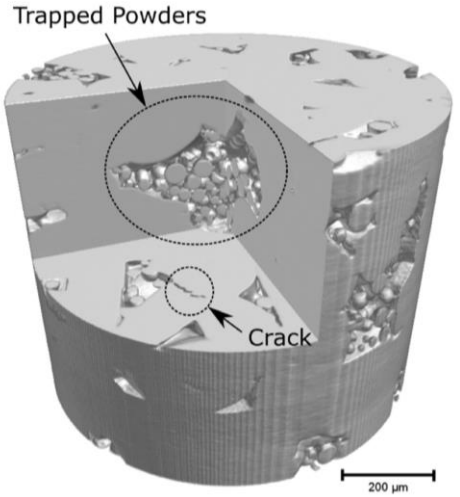

Kim, Moylan, et al., Addit. Manuf. (2017)

Entrapped gas (EG) porosity

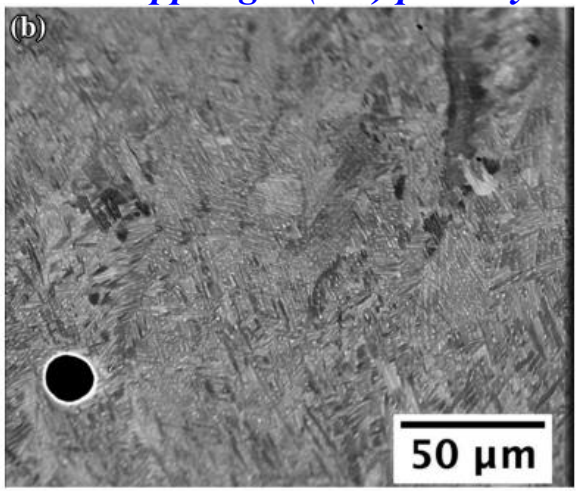

JOM, Vol. 68, No. 3, 2016 DOI: 10.1007/s11837-015-1802-0

Oxide induced porosity

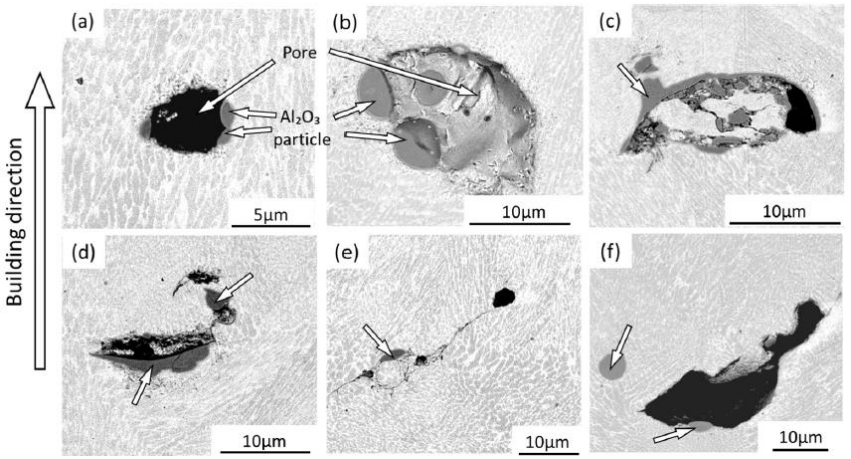

Tang et al. Int. J. Fatigue, Vol. 94, 2017, pp. 192-201

OUTLINE

- Introduction ✓
- **Process-Structure-Property (PSP) Framework**
- Effect-of-Defects Study
- Porosity Prediction Framework
- Uncertainty Quantification
- Physics-based Simulations

PSP Framework

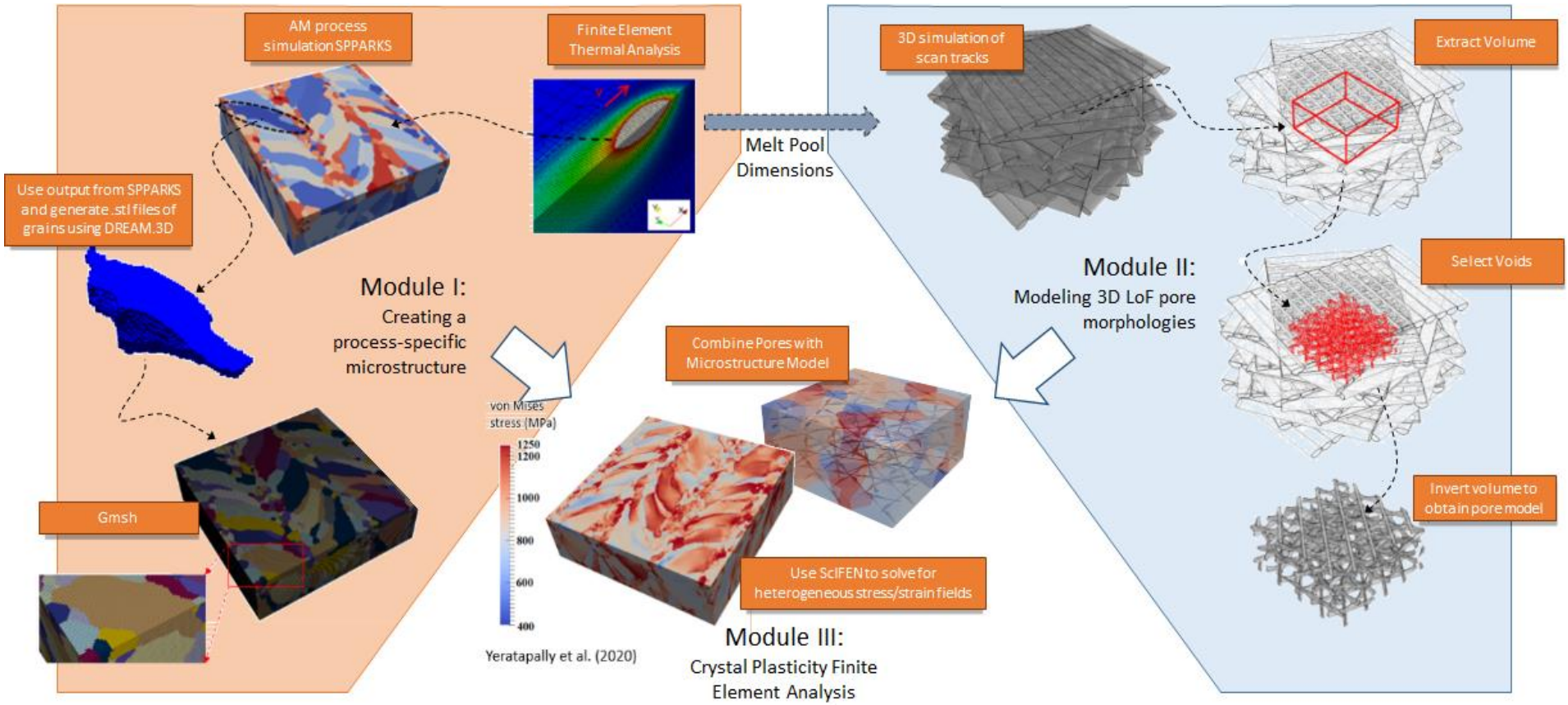

OUTLINE

- Introduction ✓
- Process-Structure-Property (PSP) Framework ✓
- **Effect-of-Defects Study**
- Porosity Prediction Framework
- Uncertainty Quantification
- Physics-based Simulations

Strain Localization Around Idealized Defect

Microstructure volume showing the location of a pore

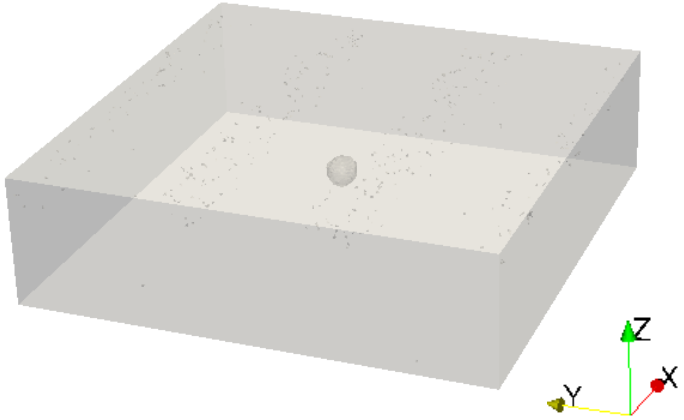

Heterogeneous strain field generated in the microstructure

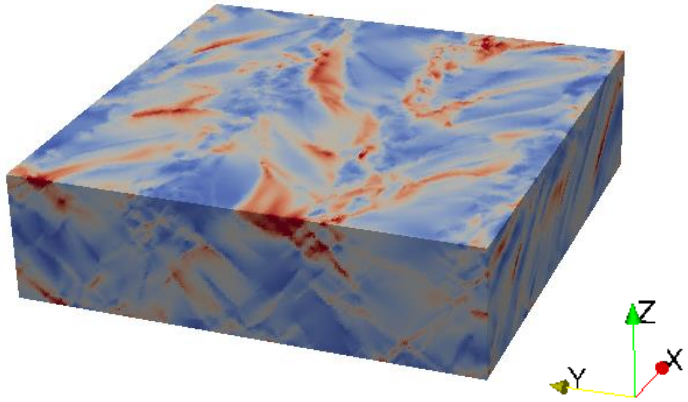

Strain field on a plane passing through the pore

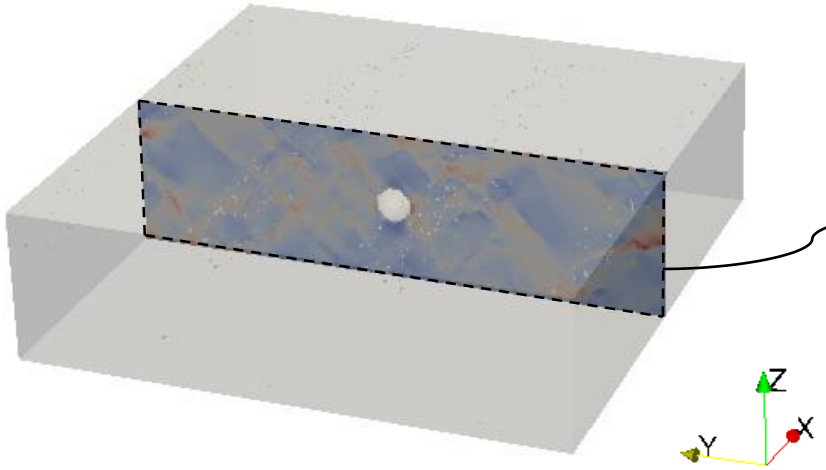

Slice view of strain field around the pore

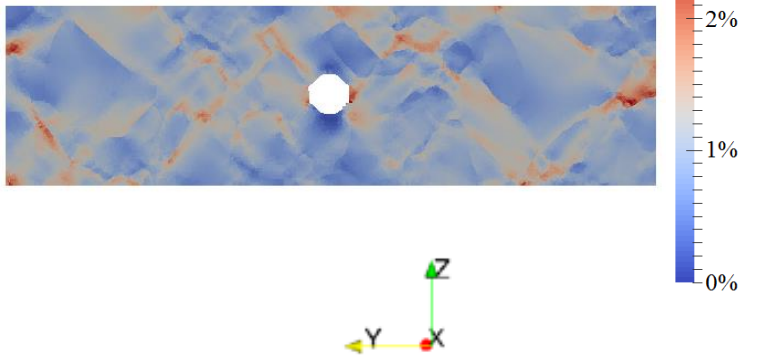

CASE STUDY: Effect-of-Defect Morphology

- Material: IN 718
- LoF (super-ellipsoids) vs. keyhole (spherical) pores
- Surrounding microstructure is the same in both cases
- Pore volume fraction is the same in both cases
- Global strain applied: 1%
- Observation: Strain localization is intense for LoF pore with sharp corners compared to the idealized keyhole pore of the same volume

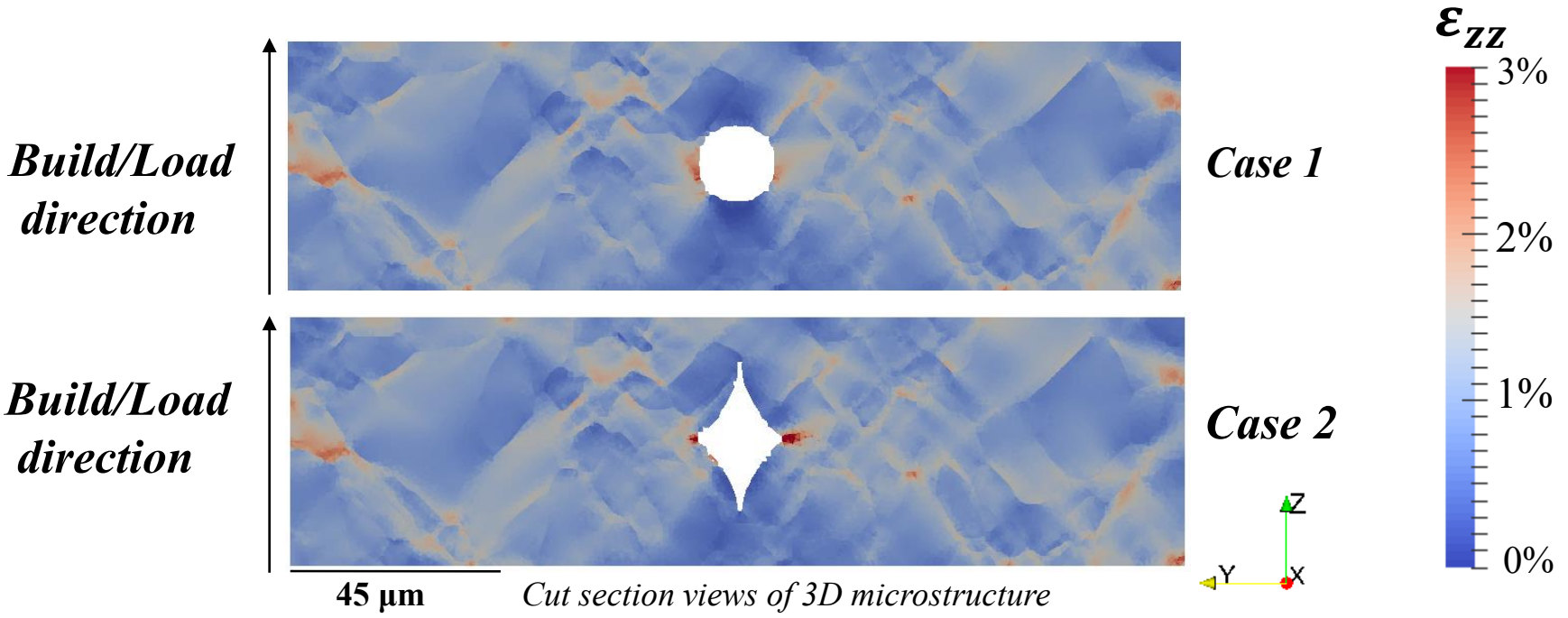

Yeratapally et al. (2020)

Cluster of Idealized Keyhole/Gas Pores

Keyhole pore distribution reconstructed from X-ray tomography

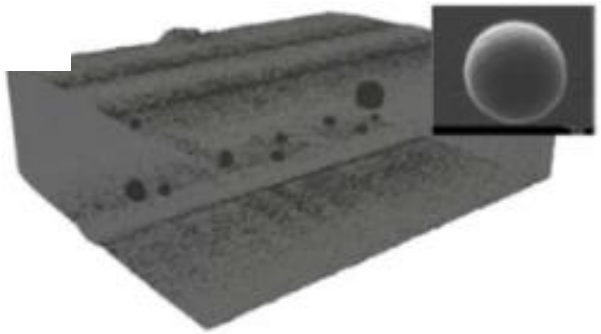

C. Panwisawas et al. / Acta Materialia 126 (2017) 251-263

3D microstructure domain showing user-specified spherical pores whose centers are collinear

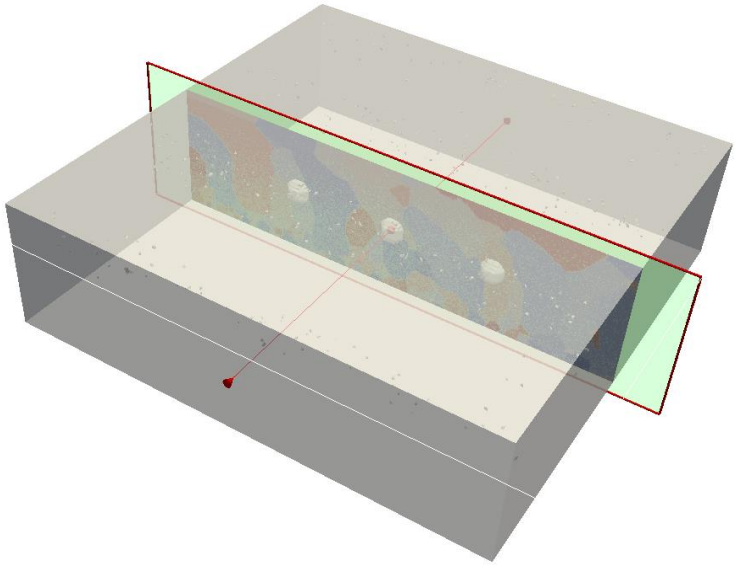

- 2D section of a 3D microstructure
- 3 cases that show varying distance between pores

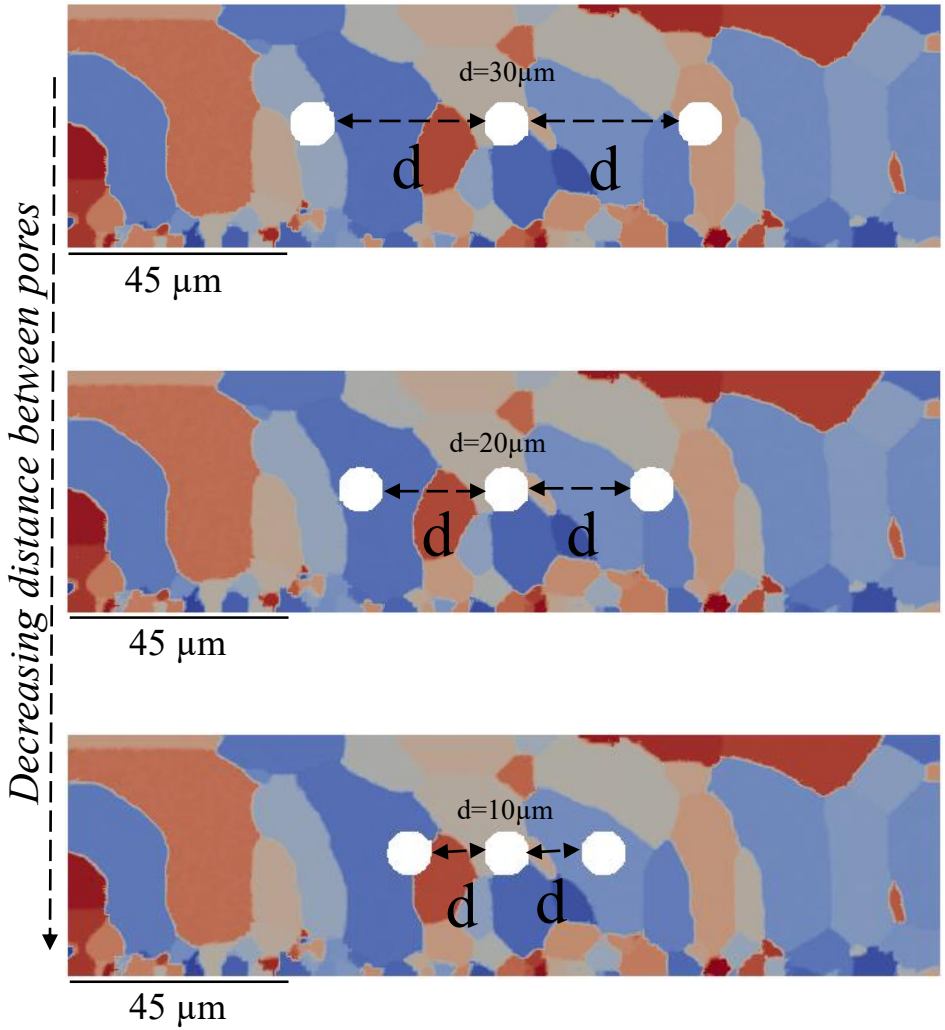

Cluster of Idealized Keyhole/Gas Pores

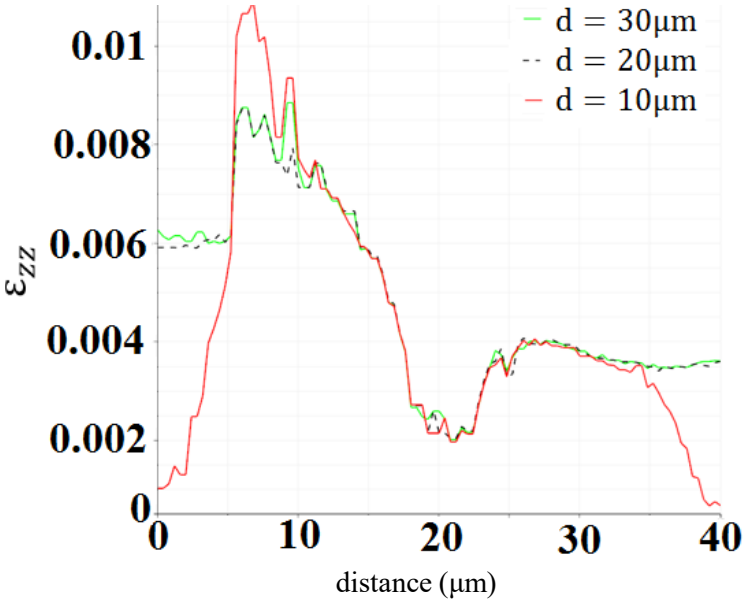

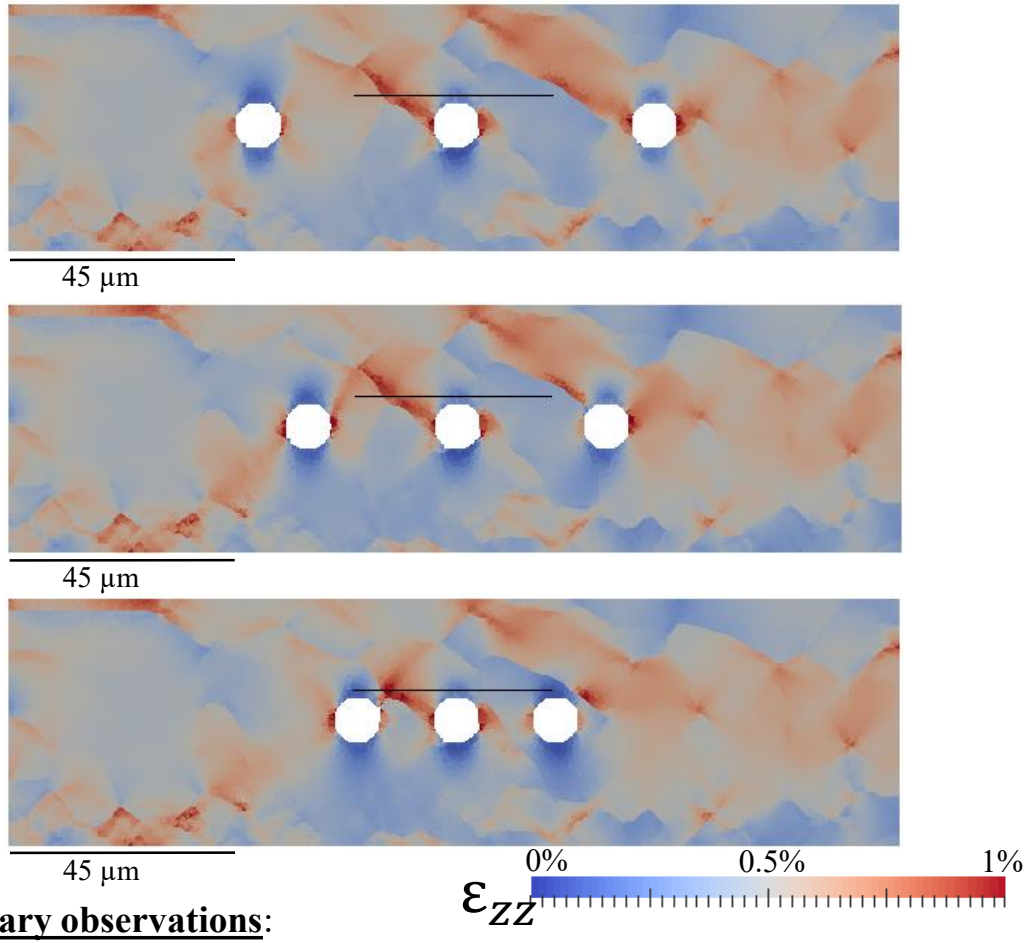

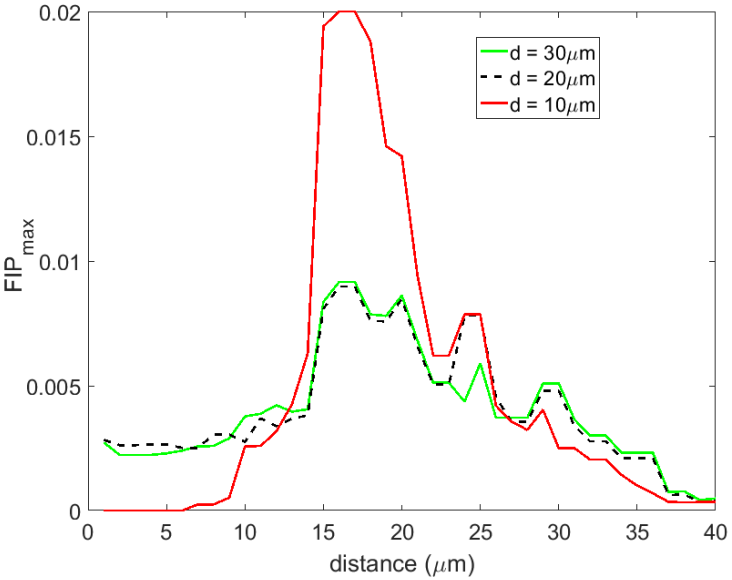

Preliminary observations:

- Strain localization at grain boundary and slip originating from the pore, interact to magnify the fatigue crack driving forces (FIP_{max}) for the case when the distance between pores is equal to the diameter of the pores (d=10μm)
- No significant effect on the strain localization (ε_{zz}) or FIP_{max} was observed for the cases d=20μm and d=30μm

OUTLINE

- Introduction ✓
- Process-Structure-Property (PSP) Framework ✓
- Effect-of-Defects Study ✓
- **Porosity Prediction Framework**
- Uncertainty Quantification
- Physics-based Simulations

LoF Porosity Prediction Framework

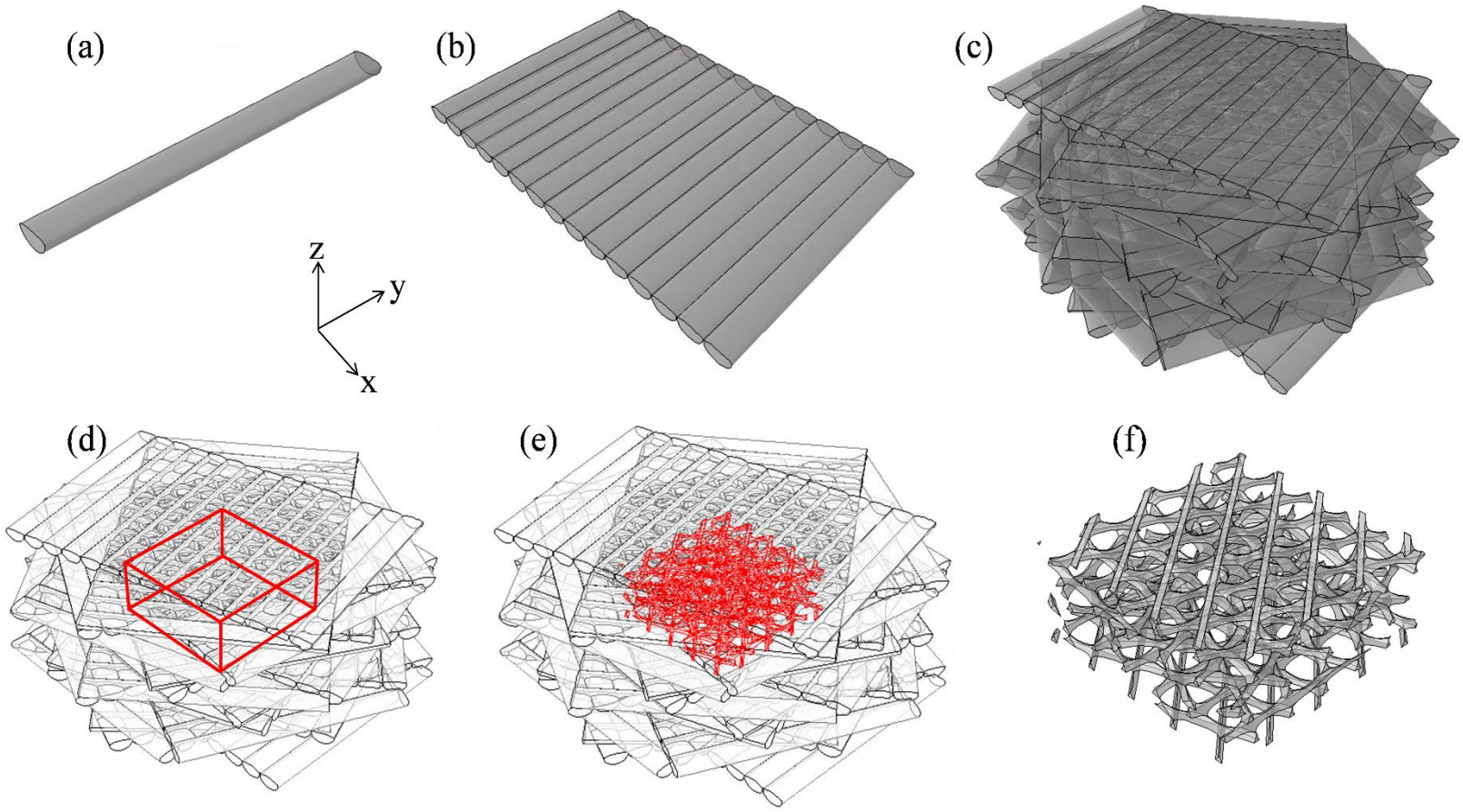

(a) An idealized scan track with a constant bi-elliptical cross section.
(b) A scan layer built by laying the scan tracks side-by-side.
(c) Multiple scan layers arranged on top of each other, each consecutive layer is rotated by hatch rotation.
(d) Box used for LoF pore extraction.
(e) LoF pore morphologies highlighted among scan tracks.
(f) Explicit morphologies of LoF pores.

Partial Validation

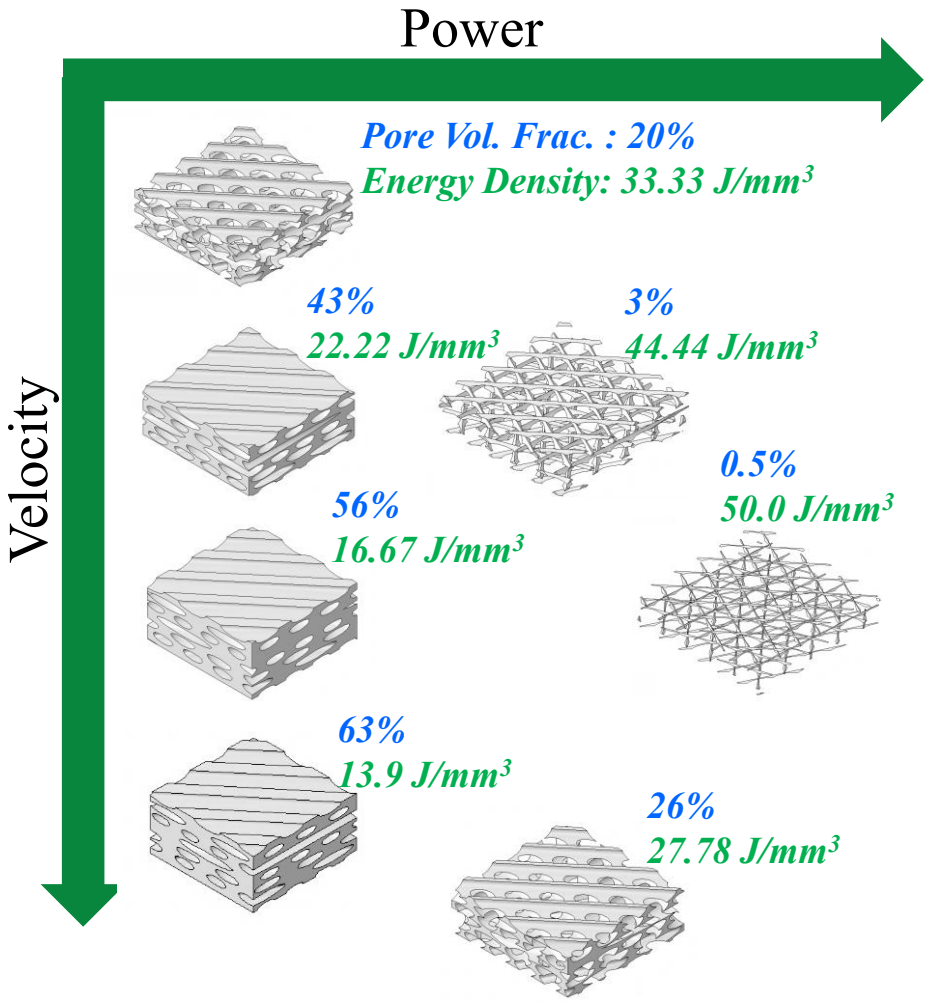

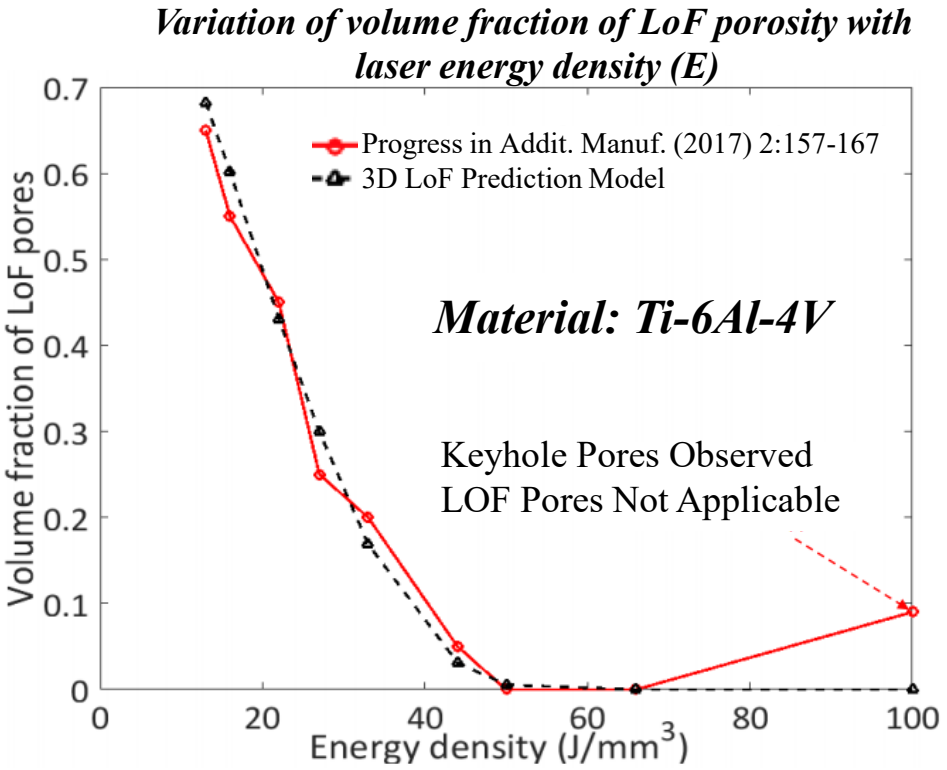

$$E = \frac{P}{VHL}$$

Process-Defect-Property Relation

- LOF pores of varying energy density.
  - explicitly modelled
  - not homogenized
- No microstructure
- Elastic-plastic, fully dense solid
  - Linear Elastic Isotropic
  - J2 plasticity
- Simple tension out to 3% strain
- Load applied in build direction

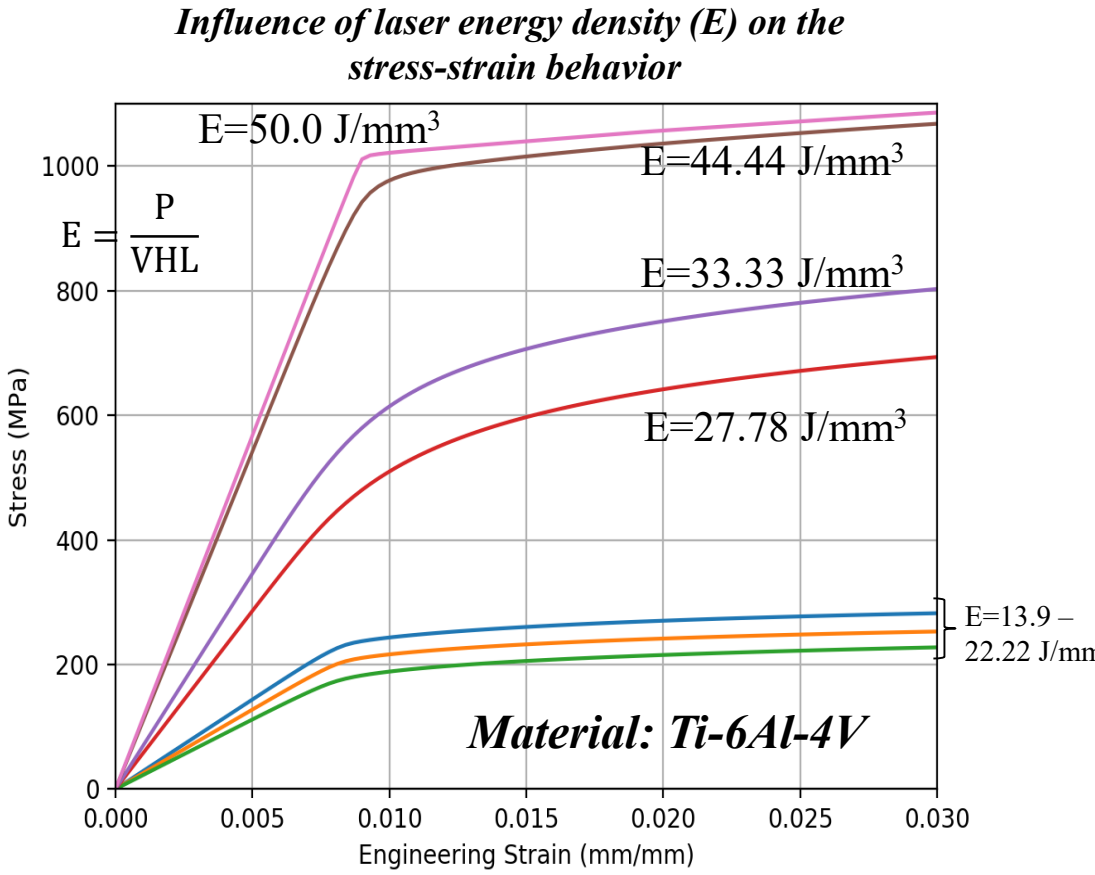

Equivalent plastic strain

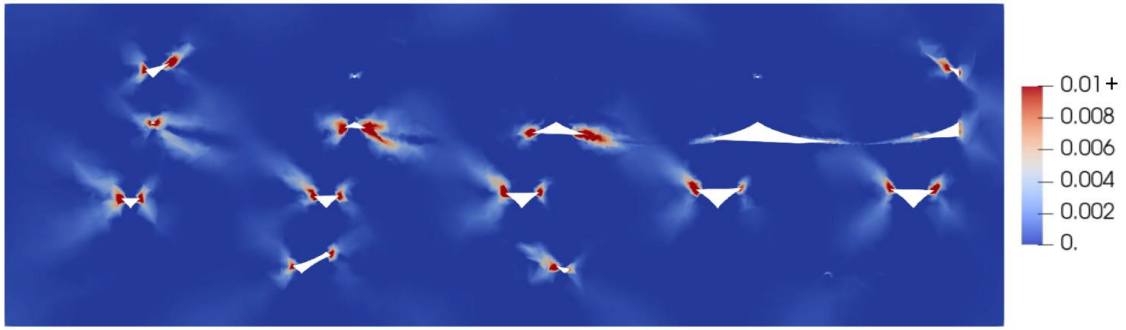

Characterization of Simulated LoF Pores

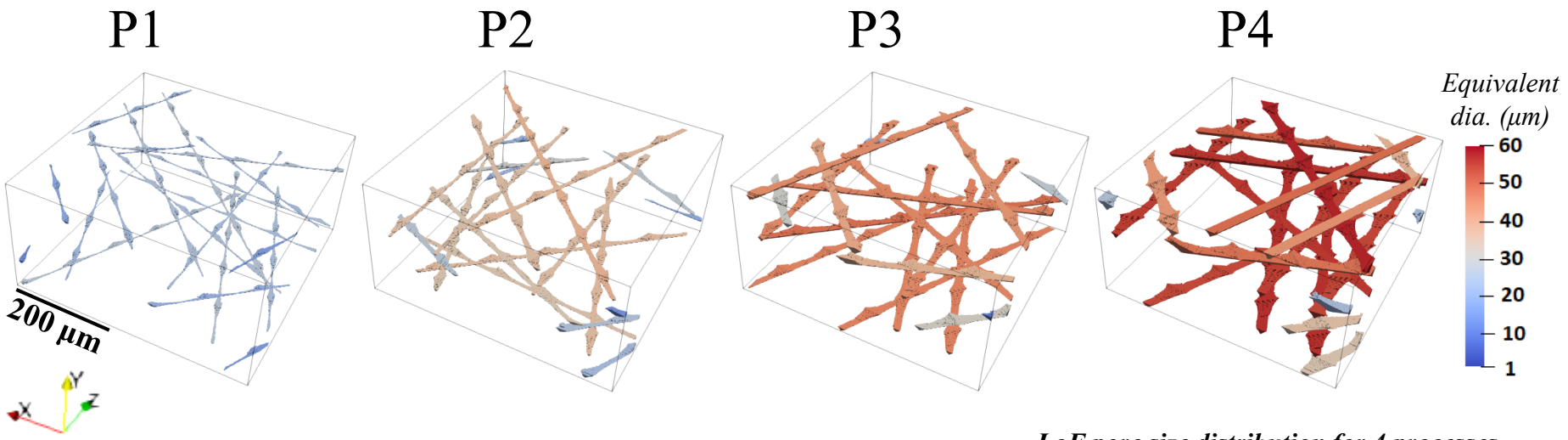

Process	P (W)	V (m/s)	E (J/mm^3)	Equ. dia (μm)
P1	150	1	50	19.75
P2	140	1	46.67	30.51
P3	100	0.75	44.44	38.96
P4	150	1.25	31.57	46.93

$$E = \frac{P}{VHL}$$

H = 100 μm
L = 30 μm
Θ = 67°

LoF pore size distribution for 4 processes (P1,P2,P3,P4)

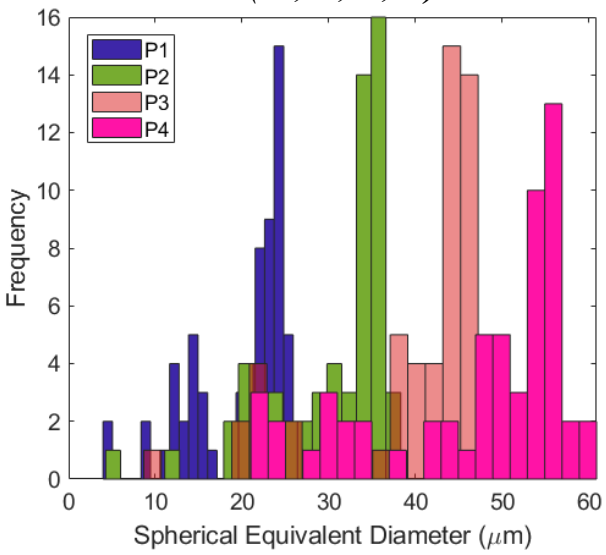

Characterization of Porosity in as-built Specimens

NASA LaRC Microfocus X-ray CT System

- X-Ray CT data will be obtained from additively manufactured Ti-6Al-4V coupons
- This data will be post-processed to characterize porosity that will in turn support the validation and development of porosity prediction models
- Specifications:
  - 5 µm Focal Spot Reflection Target X-Ray Source or 25 to 225 kV
  - 15 or 30kg Capacity 5 axis fully programmable manipulator.
  - Detector is 2000x2000 pixels with 200 micron pitch
  - 10 micron spatial resolution for specimens 1.5 cm wide
  - Thin panels 10”x10” – full volume 200 micron spatial resolution

POC: Patricia Howell

OUTLINE

- Introduction ✓
- Process-Structure-Property (PSP) Framework ✓
- Effect-of-Defects Study ✓
- Porosity Prediction Framework ✓
- **Uncertainty Quantification**
- Physics-based Simulations

Uncertainty Quantification

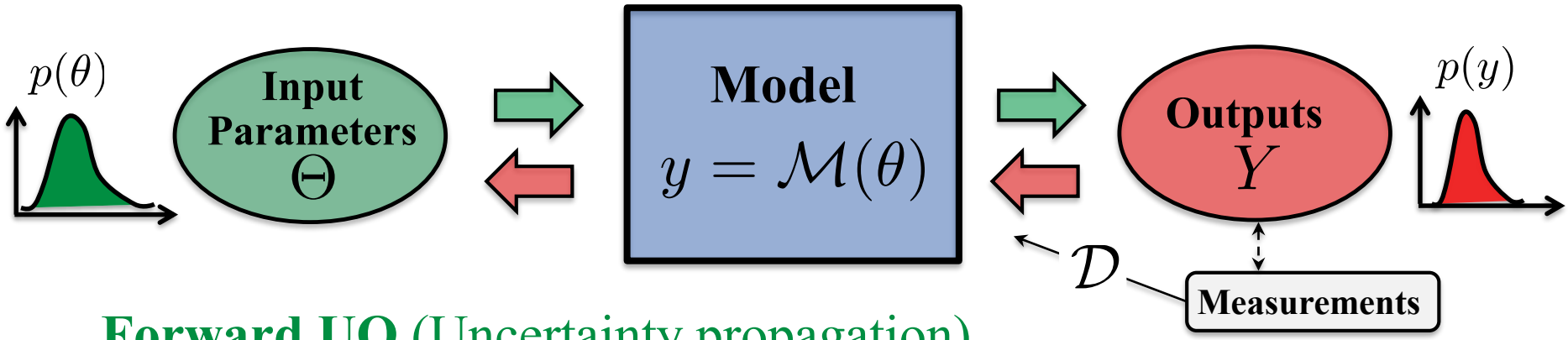

Forward UQ (Uncertainty propagation)

- **Given:** the probability distribution for the parameters, $p(\theta)$
- **Compute** the probability distribution of the outputs, $p(y)$
- **Methods:** Monte Carlo simulation, stochastic reduced order models, polynomial chaos, etc.

Inverse UQ (Probabilistic calibration or parameter estimation)

- **Given:** measured (noisy/sparse) output data, D
- **Estimate** the probability distribution of model parameters, $p(\theta|D)$
- **Methods:** Markov chain Monte Carlo, sequential Monte Carlo, etc.

Inputs

1. Epistemic Uncertainties, U

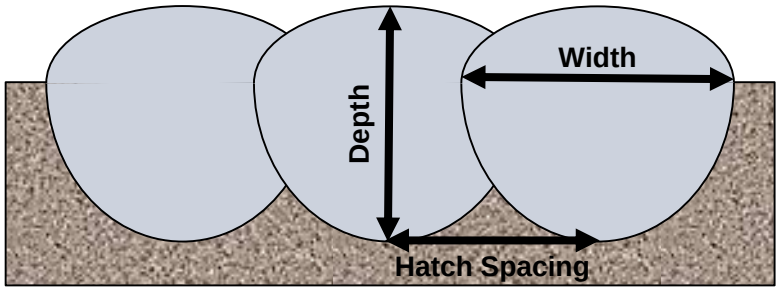

Melt pool dimensions

2. Aleatoric uncertainty, V

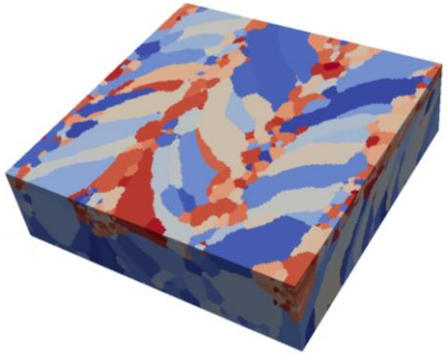

Microstructure evolution
(predicted by SPPARKS)

Output (Quantity of Interest)

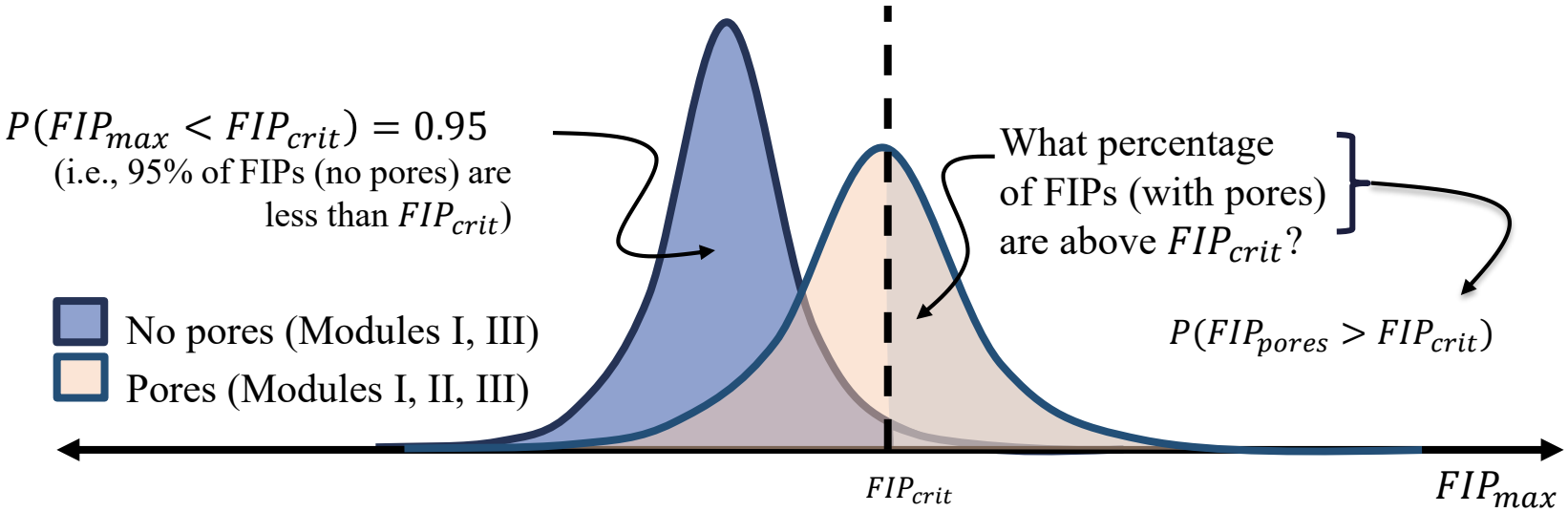

UQ Approach for the PSP Framework

- Mix of epistemic and aleatoric uncertainties creates a unique challenge
- Number of approaches [1] for dealing with this:
  - Second-order probability analysis (double-loop or two-stage Monte Carlo)
  - Interval methods
  - Dempster-Shafer evidence theory
  - ... And more
- Proposing a Two-Stage Nested Monte Carlo analysis following [1,2]

1. Swiler, Laura P., Thomas L. Paez, and Randall L. Mayes. "Epistemic uncertainty quantification tutorial." *Proceedings of the 27th International Modal Analysis Conference*. 2009.
2. Hofer, Eduard, et al. "An approximate epistemic uncertainty analysis approach in the presence of epistemic and aleatory uncertainties." *Reliability Engineering & System Safety* 77.3 (2002): 229-238.

Two-Stage Nested Monte Carlo

OUTER LOOP

Epistemic Uncertainties, U

Melt Pool Width

Melt Pool Depth

Others…

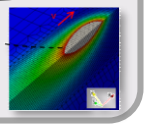

3D LoF Simulation

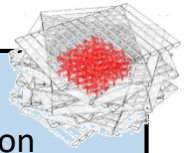

For u ~ U:
- Generate 3D LoF model
- For v ~ V:
  - Generate microstructure realization
  - Insert LoF pores into microstructure
  - Solve for QoIs

Returns: Sample-based estimate of QoI probability distributions

INNER LOOP

Aleatoric Uncertainties, V

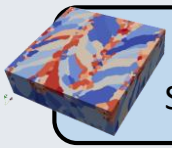

SPPARKS Simulation

3D Microstructure Model

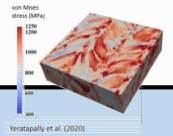

FEA Solve

Y
(Quantity of Interest e.g., FIPs)

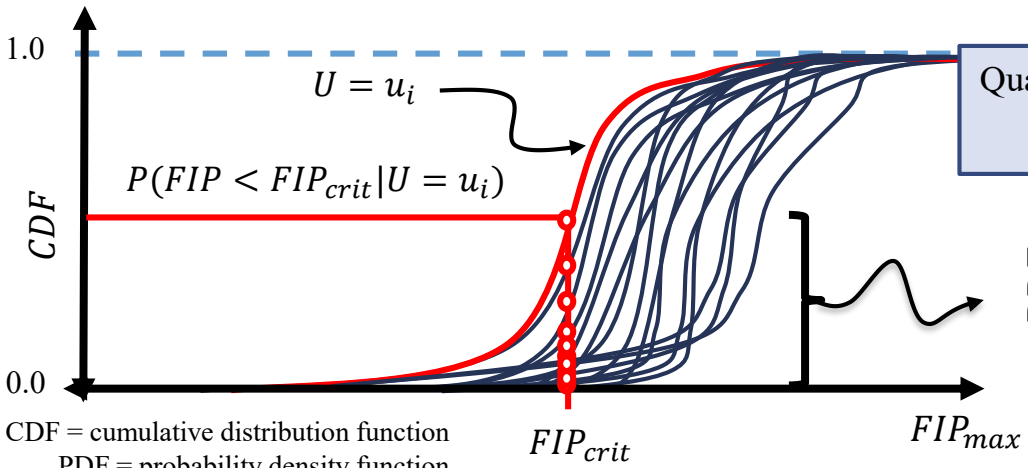

Quantity of interest:

$$P(FIP > FIP_{crit}|U) = 1 - P(FIP < FIP_{crit}|U)$$

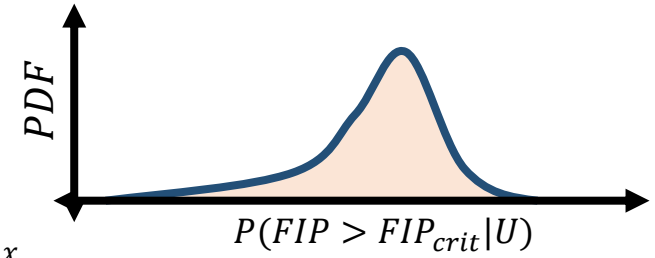

CDF = cumulative distribution function
PDF = probability density function

Accelerating the Two-Stage MC Analysis

- The quantity of interest can be computed as an expectation:

$$P(FIP > FIP_{max}|U = u) = E[Y|U = u] = E\left[1_{FIP>FIP_{max}}|U = u\right]$$

- Enables use of multi-fidelity or multi-model Monte Carlo methods [1, 2]
  - Hierarchy of faster, low-fidelity models
  - Significantly more samples of the faster models are used to supplement fewer samples of the high-fidelity model
  - Unbiased estimate of $E[Y|U = u]$
- *Takeaway:* Achieves speedup while maintaining accuracy
- Requirements:
  - Lower-fidelity model outputs must be at least weakly correlated with high-fidelity model outputs
  - More correlation the better, but speed is important

1. Gorodetsky, Alex A., et al. "A generalized approximate control variate framework for multifidelity uncertainty quantification." *Journal of Computational Physics* 408 (2020)
2. Schaden, Daniel, and Elisabeth Ullmann. "On Multilevel Best Linear Unbiased Estimators." *SIAM/ASA Journal on Uncertainty Quantification* 8.2 (2020): 601-635.

Candidates for Inner Loop Model Fusion

- Crystal plasticity fast Fourier transform (CPFFT)
  - Reduces computation time of solve
  - Los Alamos National Lab CPFFT code
- Mesh coarsening
  - Simmetrix SimModeler Voxel enables coarsening of grain mesh
- Surrogate modeling (e.g., deep learning, symbolic regression)

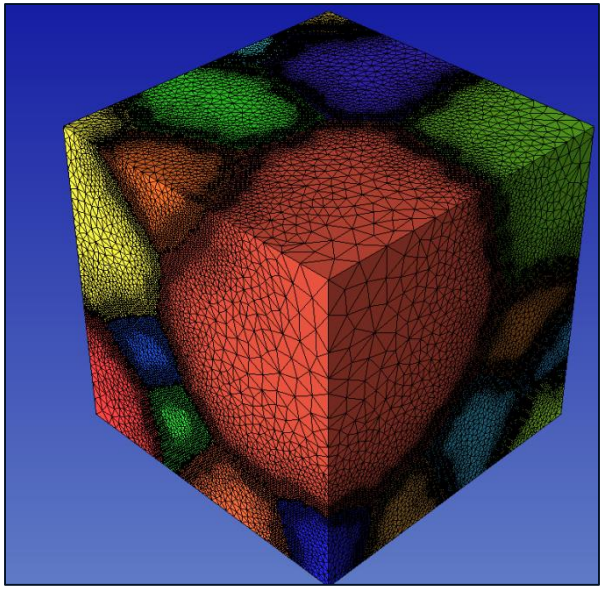

Example of grain mesh coarsening using Simmetrix SimModeler Voxel

SROM-Accelerated Outer Loop

- **SROMs** – a small number of manually selected/weighted samples

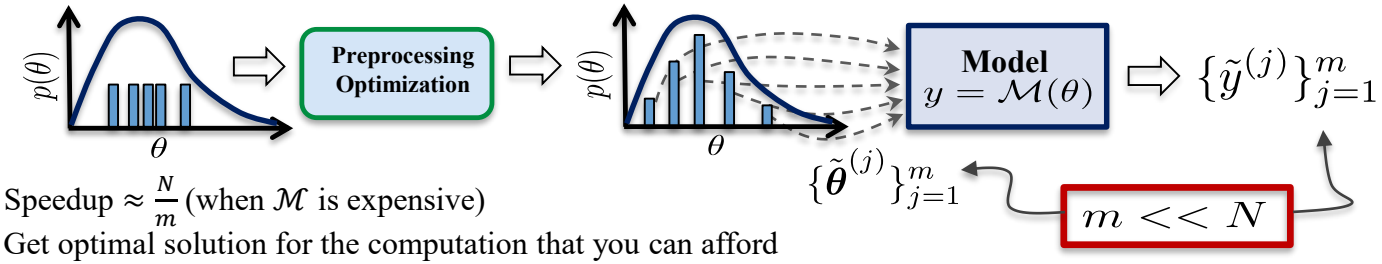

- Speedup $\approx \frac{N}{m}$ (when $\mathcal{M}$ is expensive)
- Get optimal solution for the computation that you can afford
- Proven to converge to the exact solution as m increases

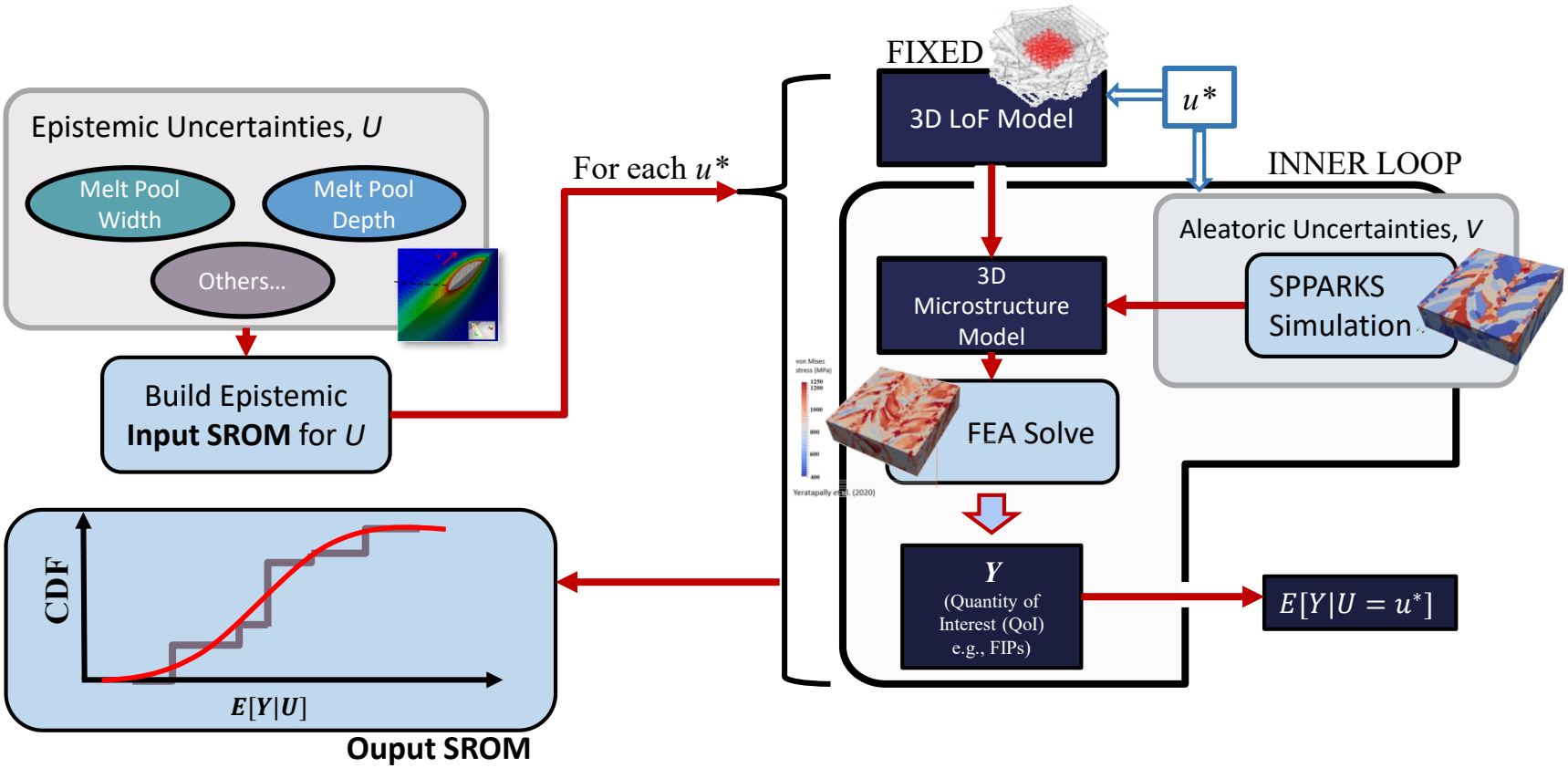

OUTLINE

- Introduction
- Process-Structure-Property (PSP) Framework
- Effect-of-Defects Study
- Porosity Prediction Framework
- Uncertainty Quantification
- **Physics-based Simulations**

Higher Fidelity Atomistic & Microstructure Simulations

Strengths & Deficiencies of Monte-Carlo Simulations

- Are able to approach macro-scales
- Simulation results seem to qualitatively agree with experiments
- Can incorporate numerous effects into model

- Fundamental physical basis lacking
- Difficult to tie to physical length/time scales
  - Makes direct coupling to thermal models more difficult
- Quantitative comparisons are less favorable

To Address Deficiencies, Utilizing Higher-Fidelity Simulations

- Atomistic simulations for thermophysical property prediction
  - Provide properties for thermal and phase-field models
- Phase-field simulations for higher-fidelity microstructure simulations
- Provide pathway forwards for validation of Monte-Carlo simulations

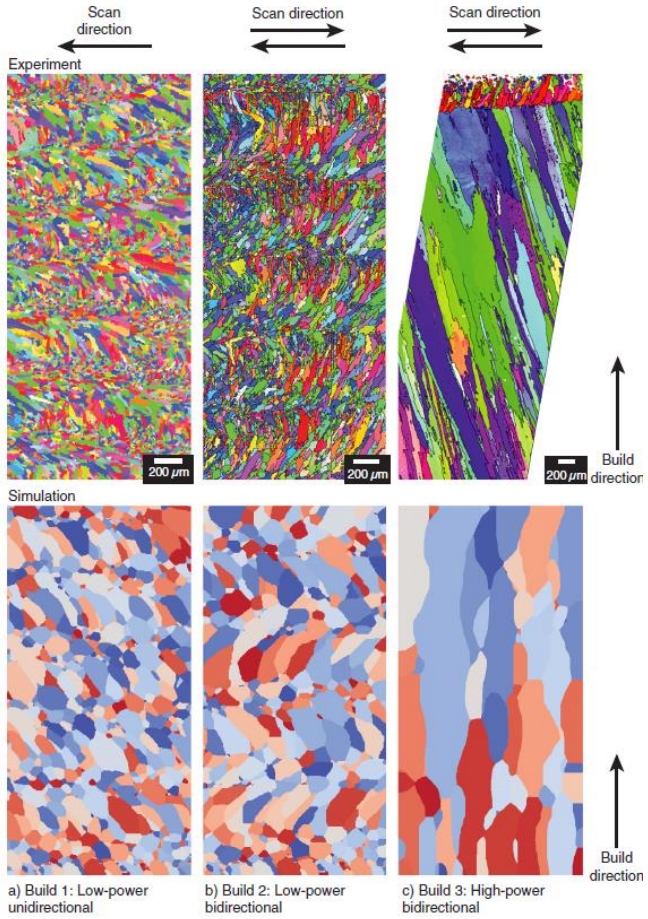

Experimental

Monte-Carlo Simulations

Rodgers, Theron M., et al. *Computational Materials Science* 135 (2017): 78-89.

The Atomistic Simulation Approach

Methods for calculating melt properties from atomistic simulations: based on statistical physics

Atomistic simulations provide raw data in terms of positions and velocities of all atoms, system energy and atomic forces

Positions: $(x_{ij}, y_{ij}, \dots)$; Velocities: $\left(v_x^{(i)}, v_y^{(i)}, \dots\right)$; Energy: $E(x_{ij}, y_{ij}, \dots)$; Forces: $f_{xi} = -\frac{\partial E(x_{ij}, y_{ij}, \dots)}{\partial x_i}$

To calculate everything else:

Virial stress: $\sigma'_{xy} = \frac{1}{N\Omega}\sum_{i\in V}\left(-m_i v_x^{(i)} v_y^{(i)} + \frac{1}{2}\sum_{j\neq i}\frac{\partial E(x_{ij}, y_{ij}, \dots)}{\partial x_{ij}} y_{ij}\right)$

Einstein-Helfand:

Diffusion: $D = \lim_{t\to\infty}\frac{1}{2t}\frac{1}{3N}\left\langle\sum_{i=1}^{N}[\vec{r}_i(t) - \vec{r}_i(0)]^2\right\rangle$

Thermal conductivity: $\kappa = \frac{1}{Vk_BT^2}\lim_{t\to\infty}\frac{1}{2t}\left\langle\left(\sum_{i=1}^{N}[\vec{G}_i(t) - \vec{G}_i(0)]\right)^2\right\rangle$;

where $\vec{G}_i(t) = [E_i(t) - \langle E_i\rangle]\vec{r}_i(t)$

Viscosity: $\eta_{xy} = \frac{1}{Vk_BT}\lim_{t\to\infty}\frac{1}{2t}\left\langle[\Psi_{xy,i}(t) - \Psi_{xy,i}(0)]^2\right\rangle$;

where $\Psi_{xy,i}(t) = \sum_{i=1}^{N} m_i v_{x,i}(t) y_i(t)$

Green-Kubo:

$D = \frac{1}{3N}\int_0^\infty\left\langle\sum_{i=1}^{N}\vec{v}_i(t) * \vec{v}_i(0)\right\rangle dt$

$\kappa = \frac{1}{Vk_BT^2}\int_0^\infty\langle\vec{J}(t) * \vec{J}(0)\rangle dt$; $\vec{J}(t) = \frac{d\vec{G}(t)}{dt}$

$\eta_{xy} = \frac{1}{Vk_BT}\int_0^\infty\langle P_{xy}(t)P_{xy}(0)\rangle dt$; $P_{xy}(t) = \frac{d\Psi_{xy,i}(t)}{dt}$

Liquid-vacuum and solid-liquid interface tension:

Capillary pressure method: $\gamma = \frac{pL}{2}$

Capillary fluctuation method: $\gamma = \frac{k_BT}{A\langle|A(k)|^2\rangle k^2}$

$A(k)$ - capillary fluctuation as a function of the wave vector, k.

Require large statistics from long and precise simulations

Melt Properties of Pure Al and Ti

Aluminum: MD-PINN[1] vs DFT[2] vs Experiment[2]

Titanium: MD-EAM[3] vs Experiment[4]

Diffusivity, Al

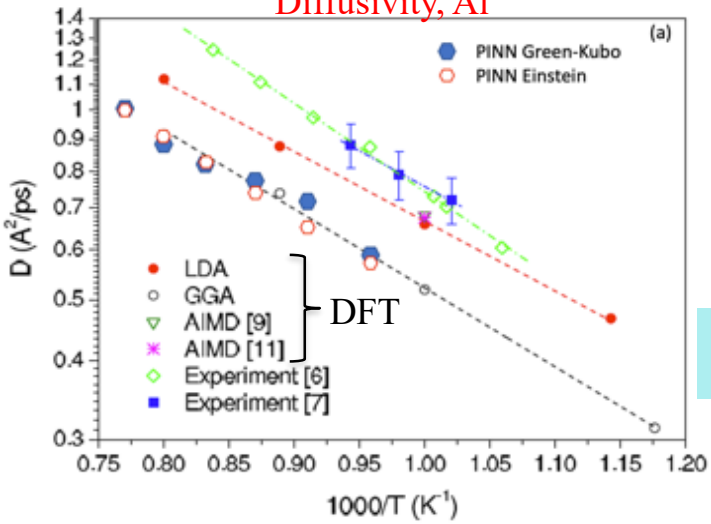

Surface Tension, Al

Capillary fluctuation method: $\gamma = 0.610\ J/m^2$

Capillary pressure method: $\gamma = 0.613\ J/m^2$

Experiment: $\gamma = 0.87\ J/m^2$

Al: MD-PINN matches GGA-DFT used to train the NN
Ti: MD-EAM shows weaker match to Experiment

Diffusivity, Ti

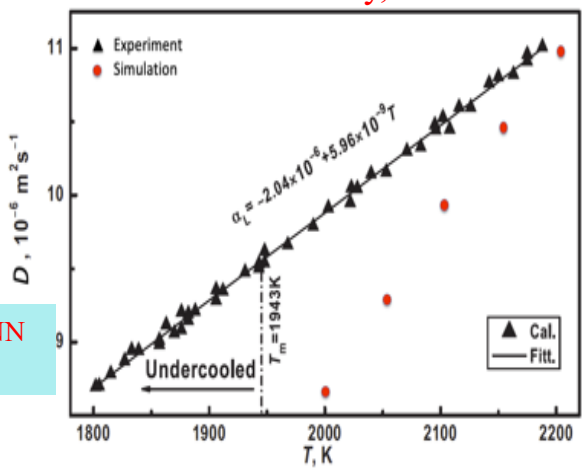

Viscosity, Al

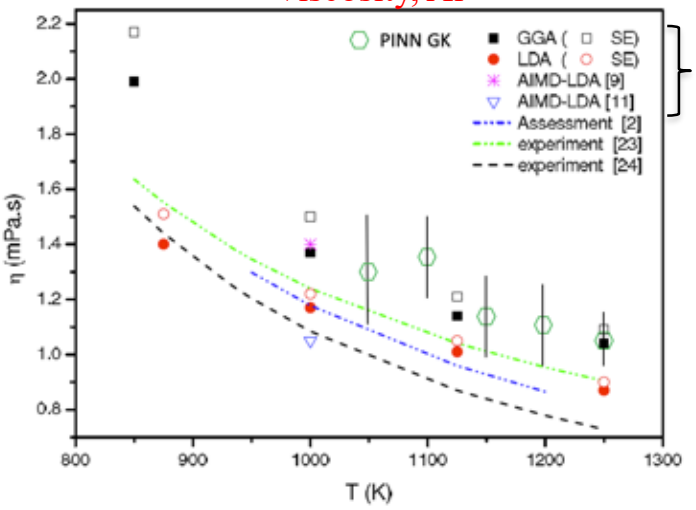

Viscosity, Ti

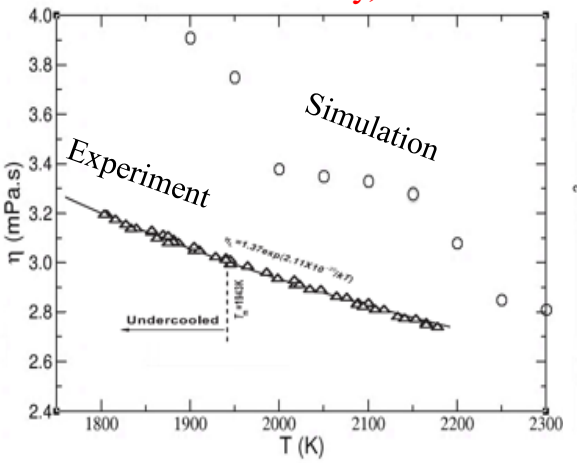

Surface tension, Ti

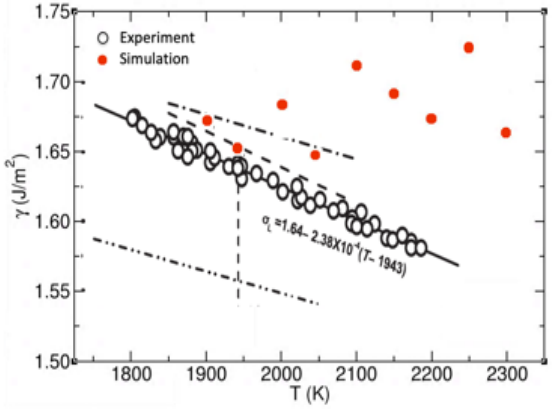

[1]G.P.Purja Pun et al., Nature Comm. (2019) 0:2339. DOI: 10.1038/s41467
[2]N. Jakse, A. Pasturel, Sci. Rep. (2013) 3:3135. DOI: 10.1038/snep03135
[3]M.I.Mendelev et al., J.Chem.Phys. 145 (2016) 154102. [4]K. Zhou et al. Chem. Phys. Letts. 639 (2015) 105-108.

Phase-Field Modeling of AM

Phase Field (PF) Modeling

- Technique for simulating a range of microstructural phenomena
  - Solidification, grain growth, precipitation, decomposition, etc.
- Cahn-Hilliard Diffusion Equation (Conserved quantities)

$$\frac{\partial c}{\partial t} = \nabla \cdot \left(M \nabla \frac{\delta F}{\delta c} \right)$$

- Allen-Cahn Relaxation Equation (Non-conserved quantities)

$$\frac{\partial \phi_i}{\partial t} = -L \frac{\delta F}{\delta \phi_i}$$

- Free Energy Functional (energy of system)

$$F = \int \left[f_{chem} + f_{grad} + f_{mech} + f_{ext} \right] dV$$

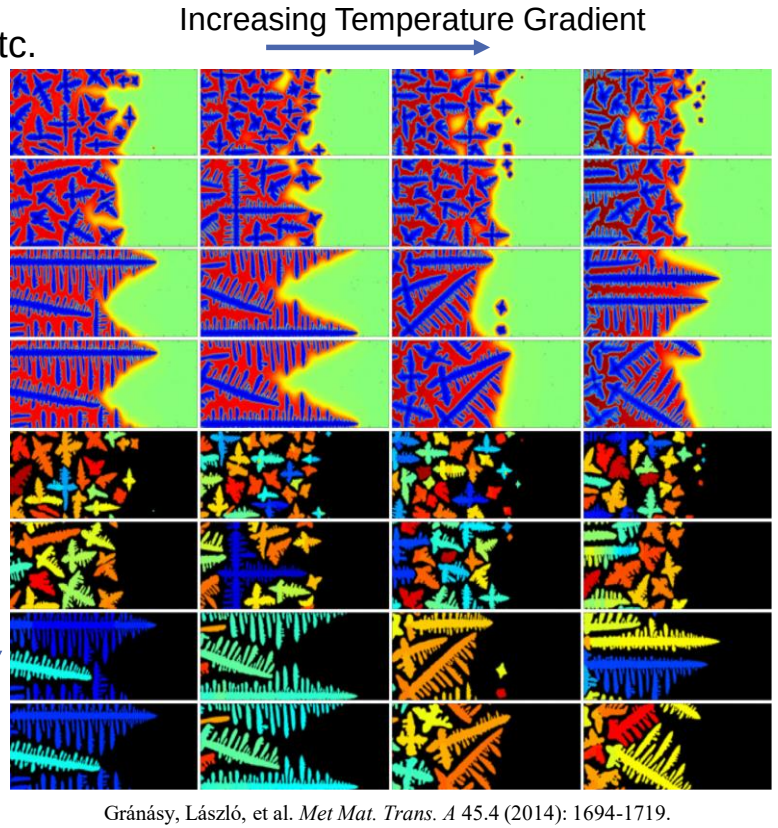

Gránásy, László, et al. *Met Mat. Trans. A* 45.4 (2014): 1694-1719.

Anticipated Benefits

- Provide high-fidelity simulations to validate Monte-Carlo results
  - Dendritic tip velocity, orientation/texture, grain size
- Provide additional details not captured in Monte-Carlo methods
  - Alpha-beta transition, dendritic arm spacing, solute trapping

Acknowledgements

This work is currently being funded by the NASA Aeronautics Research Mission Directorate's Transformative Tools and Technologies (TTT) project

Thank you!